Natural convection in a side-facing open cavity

H. Skok, S. Ramadhyani, and R. J. Schoenhals
Ray W. Herrick Laboratories, School of Mechanical Engineering, Purdue University, West Lafayette, IN, USA

A combined experimental and numerical study of buoyancy-driven flow in a side-facing open cavity was conducted. Such flows occur in household refrigerators and ovens under open-door conditions and also in the cavities of solar central receivers. In this study, a two-dimensional numerical simulation was employed to predict the flow pattern in the cavity and both local and average Nusselt numbers for the surfaces of the cavity. The experiments provided an assessment of the accuracy of the predicted average Nusselt numbers in the Rayleigh number range in which the numerical and experimental studies overlapped. Visual observation of the flow in the experimental apparatus indicated qualitative agreement with the predicted flow pattern, although the three-dimensionality of the flow could not be predicted by the simulation. Correlating equations were developed for the surface-average and cavity-average Nusselt numbers based on the experimental and numerical results.

Keywords: open cavity; refrigerator door opening; natural convection; solar central receivers

Introduction

When the walls of a side-facing open cavity are maintained at a temperature different from that of the ambient fluid, a buoyancy-driven flow is generated. Figure 1 is a schematic depiction of such a flow. The walls of the cavity are at a uniform temperature T_w, and the opening of the cavity faces a large quiescent body of fluid at temperature T_∞. If T_∞ exceeds T_w, cold fluid from within the cavity flows out near the bottom while warm ambient fluid flows in near the top. Such flows occur in household refrigerators and ovens under open-door conditions and also in the cavities of solar central receivers.

This article describes a combined experimental and numerical study of fluid flow and convective heat transfer in a side-facing open cavity. The study was undertaken as part of a larger investigation of heat and mass transfer into the cooled space of a conventional household refrigerator. Attention was directed at door openings, which were suspected of contributing appreciably to the overall energy transfer into the refrigerator. With reference to Figure 1, the dimensions of the fresh-food compartment of a typical domestic refrigerator are $H=0.90$ m and $D=0.60$ m. The width of the cavity (dimension perpendicular to the plane of the figure) is typically $W=0.75$ m. The associated Rayleigh number for the buoyancy-driven flow is approximately 10^9.

The present experimental studies were undertaken in a model cavity with an aspect ratio, $H/D=1.5$, similar to that of the fresh-food compartment of a refrigerator. By using glycerol–water mixtures of different compositions as the working fluid, a wide range of Rayleigh numbers was achieved while keeping the temperature difference between the hot and cold surfaces essentially constant. The experiments were supplemented with a two-dimensional (2-D) numerical study and, where possible, experimental and numerical results were compared.

Address reprint requests to Professor Ramadhyani at the School of Mechanical Engineering, Purdue University, West Lafayette, IN 47907, USA.

Received 11 January 1990; accepted 1 October 1990

Literature review

Studies on solar central receiver cavities have been reported by Boehm,[1] Siebers *et al.*,[2] Clausing,[3] and Kraabel.[4] The flow conditions in solar central receivers are characterized by high Rayleigh numbers, well into the turbulent range, and large temperature differences, which result in large variations of fluid properties. The geometries are not always simply rectangular and may involve baffles covering part of the opening. Actual operating conditions involve forced flows as well, in the form of wind impinging on the receiver. Experiments conducted on actual receiver setups, therefore, do not always represent pure free convection conditions. Empirical correlations for the cavity-average Nusselt number have been presented by Clausing and Kraabel.

Laboratory experimental studies have been reported by Chan and Tien,[5] Hess and Henze,[6] Sernas and Kyriakides,[7] Chen

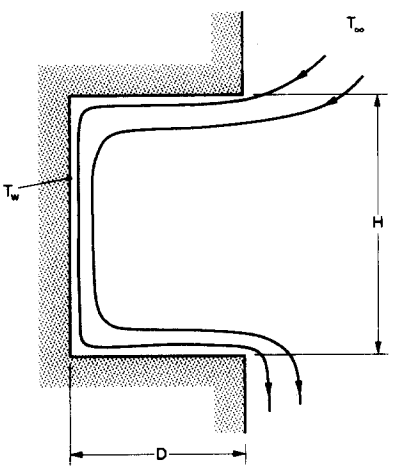

Figure 1 Schematic depiction of buoyancy-driven flow in a side-facing open cavity

et al.,[8] and Chen *et al.*[9] In the studies by Chan and Tien and Hess and Henze, only the back wall of the cavity was heated while the top and bottom walls were adiabatic. In the Sernas and Kyriakides study, the top and back walls were heated while the bottom wall was at ambient temperature. In the study by Chen *et al.*[8] all three walls were heated, while in the study by Chen *et al.*[9] the bottom and back walls were directly heated, and the top wall was allowed to achieve its own equilibrium temperature dictated by heat transfer from the other two walls.

Chan and Tien investigated a very narrow cavity, with an aspect ratio (H/D) of only 0.143. Their study encompassed both flow field and heat transfer measurements, but the differences in geometry and thermal boundary conditions limit the applicability of those results to the present situation. In like vein, differences in experimental methods and boundary conditions limit the applicability of the results generated by Hess and Henze. Sernas and Kyriakides used a Wollaston prism schlieren interferometer to measure the temperature gradient locally at the heated surfaces of the cavity and thus determine local heat transfer coefficients. Although those results are of qualitative interest to the present investigation, quantitative comparisons are restricted by the difference in thermal boundary conditions.

Chen *et al.*[8] have reported the results of a flow visualization study of the heated open cavity. Various cavity orientations were examined, and in some cases, the flow was observed to be pulsatile. A very detailed study of the open cavity, under both free convection and mixed convection conditions has been reported by Chen *et al.*[9] Velocity, temperature, and turbulence intensity measurements have been made for several cavity aspect ratios and orientations. However, no heat transfer measurements were reported from that study.

Numerical studies of natural convection in open cavities have been presented by Chan and Tien,[10,11] Penot,[12,13] LeQuere *et al.*,[14] and Humphrey and To.[15] In each of these studies, the flow field was assumed to be 2-D. In the studies by Chan and Tien, the back wall of the cavity was prescribed to be at a uniform temperature exceeding that of the ambient, while the other two walls were adiabatic. In the other studies, all three walls were at a uniform temperature exceeding the ambient. The calculations performed by Humphrey and To correspond to turbulent natural convection conditions and involve the use of a low Reynolds number turbulence model, whereas the other studies correspond to laminar natural convection.

The imposition of boundary conditions was a common problem in each of the aforementioned numerical studies. Clearly defined boundary conditions exist only inside and close to the cavity itself, while other boundaries are found far removed from the cavity opening at "infinity." In order to keep the grid size within manageable limits, these large surroundings have to be ignored, and boundary conditions that would properly represent the influence of a semi-infinite quiescent medium have to be imposed at the actual boundaries of the computational domain.

The solution chosen by all the foregoing investigators in dealing with this problem was to keep the far boundaries at a large enough distance from the cavity that uncertainties in the boundary conditions at those surfaces would not influence the flow and heat transfer conditions inside, and close to, the cavity. LeQuere *et al.* determined the sensitivity of the solution in the cavity region on the conditions at the far boundaries by performing calculations with different locations of the far boundaries and different sets of boundary conditions. In general, the flow and temperature fields inside the cavity were found to be insensitive to the precise details of the boundary conditions at "infinity."

Experimental procedure

The test apparatus consisted of a large Plexiglas tank in which a side-facing, open, rectangular cavity was constructed, as shown in Figure 2. The width of the cavity, W, was 0.305 m. The top, back, and bottom walls of the cavity were made of aluminum plates, 12.7 mm thick, with electrical strip heaters glued to the back of each plate to elevate the plate surface temperature above the fluid temperature. Glycerol–water mixtures of different compositions were used as the working fluid. To absorb the heat transferred at the cavity walls and maintain constant fluid

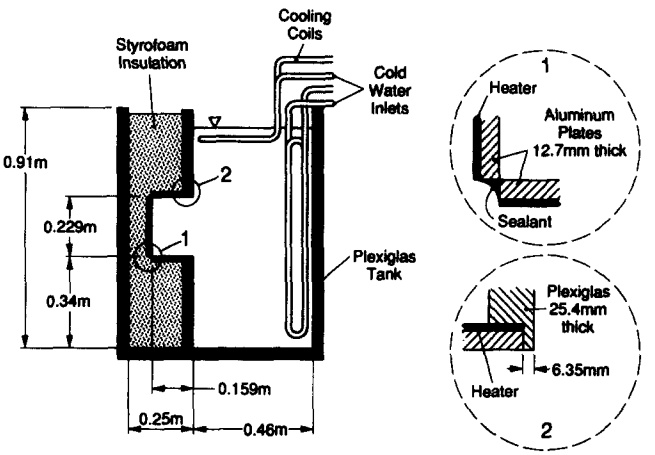

Figure 2 Schematic of the test apparatus

Notation

A	Surface area of a heated plate
c_p	Specific heat at constant pressure
D	Depth of the cavity
H	Height of the cavity
k	Thermal conductivity of the fluid
L	Characteristic length employed in heat transfer correlations for free convection on horizontal flat plates
Nu_H	Local Nusselt number, Equation 13
$\overline{\mathrm{Nu}}_H$	Plate average Nusselt number, Equation 2
P	Perimeter of horizontal flat plate
$\hat{p}$	Reduced pressure, Equation 9
Ra_H	Rayleigh number, Equation 3
T_w	Temperature of the heated walls
T_c	Temperature of the cold surface
u, v	Velocity components in the x and y direction, respectively
u_{max}	Maximum outflow velocity in the mouth of the cavity opening
W	Width of the cavity
x, y	Coordinate directions

Greek symbols

β	Coefficient of thermal expansion of the fluid
μ	Dynamic viscosity of the fluid
ν	Kinematic viscosity of the fluid
ρ	Fluid density

temperature, copper cooling coils were installed at the top of the tank and adjacent to the vertical side wall facing the cavity opening. Thus a buoyancy-driven flow could be generated and sustained in the test cell.

In establishing the dimensions of the test cell, the volume of the liquid reservoir facing the cavity was made as large as possible, within practical limits, to simulate a semi-infinite quiescent medium. Preliminary studies involving both flow visualization and temperature measurements revealed that the bulk of the liquid in the reservoir was mostly quiescent and isothermal to within about 1°C while the experiments were being run. There were, of course, significant velocities and temperature variations in the boundary layers adjacent to the cooling coil surfaces. In addition, the liquid below the lower lip of the cavity was observed to be thermally stratified. However, the conditions of the experiment are believed to be a reasonable approximation to an isothermal open cavity facing a large quiescent medium.

Care was taken to provide good insulation between the plates, as well as between the plates and the surroundings, by insulating the backs of the plates with Styrofoam and mounting the plates in the sidewalls of the tanks with nylon bolts. At the corners, the plates touched only along their edges (see detail 1 in Figure 2), and the edges of the plates facing the fluid were covered by the lip of the Plexiglas partition (see detail 2 in Figure 2). These precautions ensured that heat transfer from the plates occurred mainly through the three heated surfaces of the cavity, and extraneous heat losses were small. The entire tank was well insulated with Styrofoam so that heat losses through the tank walls were negligibly small.

Plate surface temperatures were measured with calibrated copper-constantan thermocouples inserted through holes drilled into the backs of the plates. The thermocouple junctions were located 0.8 mm from the surfaces of the plates. A 3×3 array of thermocouples was used on each plate to register surface temperatures. The surface temperatures of the cooling coils were measured by eight additional thermocouples attached at various locations. The estimated uncertainty in temperature measurements is ± 0.1 K.

The strip heaters attached to the backs of the plates were electrically connected in pairs. Two pairs were mounted on the bottom plate, two on the top plate, and three on the back plate, so that the back surface of each plate was completely covered by the heaters. Each pair of heaters was connected to an autotransformer. Adjusting the heater voltages appropriately kept the surface temperatures on each plate uniform within 5 percent of the driving temperature difference between the plates and the cooling coil. This temperature difference was maintained at about 8 K in all the tests to limit fluid property variations with temperature. The power dissipated in each pair of heaters was measured by a watt transducer accurate to within 0.1 percent of the full-scale reading of 200 W.

In order to cover a wide range of Rayleigh numbers, different mixtures of glycerol and deionized water were used. For the limiting cases of pure glycerol (99.5 percent, USP-grade) and pure water, the associated Rayleigh numbers were 3.5×10^6 and 1.2×10^9, respectively. Several tests were conducted with each working-fluid mixture, with good repeatability between the tests. The composition of each glycerol–water mixture was determined by measuring its density and using the tabulated values for the specific gravity of mixtures of glycerol and water given by Miner and Dalton.[16] The other thermophysical properties of the mixtures were obtained from the same source.

The characteristic length for both the Rayleigh number and the Nusselt number was chosen as the cavity height H. The characteristic temperature difference, ΔT, was the difference between the surface temperatures of the heated plates and the cooling coils:

$$\Delta T = T_w - T_c \tag{1}$$

The average Nusselt number for each plate was calculated as:

$$\overline{\mathrm{Nu}}_H = \frac{P}{A}\frac{H}{\Delta T\, k} \tag{2}$$

with A being the plate surface area and P the electric power dissipated in the heaters attached to the plate. The Rayleigh number was determined from the expression:

$$\mathrm{Ra}_H = \frac{g\rho^2\beta\,\Delta T\, H^3 c_p}{\mu k} \tag{3}$$

All property values were evaluated at the film temperature:

$$T_f = 0.5(T_w + T_c) \tag{4}$$

Detailed error estimates associated with the various measured and derived quantities are given by Skok.[17] The overall uncertainty in the determination of the Rayleigh number is estimated to be ± 12 percent in the worst case (pure glycerol) and ± 6 percent in the best case (pure water). For the Nusselt number, the errors in the determination of the temperature difference and plate heat transfer rate combine to yield potential overestimates of between 2 percent and 5.5 percent for the back and bottom plates and between 5.5 percent and 25 percent for the top plate. The higher uncertainties are associated in each case with the lowest Rayleigh number.

The uncertainty in the Nusselt number for the top plate is much higher than for the back and bottom plates because, to maintain isothermal conditions, a much lower power dissipation is required in the top plate heaters than in the other two plates. Therefore the uncertainty in the power measurement results in a much higher relative uncertainty in the top plate Nusselt number.

In addition to the heat transfer measurements, flow visualization studies were conducted in the test cell using the electrochemical thymol blue technique.[18] Pure water was used for these studies, the associated Rayleigh number being 1.5×10^9. By positioning the cathode at different locations in the test cell and observing the streaks of color emanating from it, a qualitative impression of the general features of the flow was obtained. Although still-frame photographs of the dye streaks were taken, the low contrast level in these photographs rendered them unsuitable for presentation.

Mathematical model

The geometry of the calculation domain was chosen to be similar to that of the test cell, but only 2-D variations in the x and y directions were considered in the model; variations in the z direction were neglected (Figure 3). Under the assumptions that the fluid was Newtonian, viscous dissipation and work of compression were negligible, the flow was steady, and density variations were negligible except in the body force term (Boussinesq approximation), the governing equations of continuity, momentum, and energy were formulated in 2-D Cartesian coordinates:

$$\frac{\partial u}{\partial x} + \frac{\partial v}{\partial y} = 0 \tag{5}$$

$$\rho\left(u\frac{\partial u}{\partial x} + v\frac{\partial u}{\partial y}\right) = -\frac{\partial \hat{p}}{\partial x} + \mu\left(\frac{\partial^2 u}{\partial x^2} + \frac{\partial^2 u}{\partial y^2}\right) \tag{6}$$

$$\rho\left(u\frac{\partial v}{\partial x} + v\frac{\partial v}{\partial y}\right) = -\frac{\partial \hat{p}}{\partial y} + \mu\left(\frac{\partial^2 v}{\partial x^2} + \frac{\partial^2 v}{\partial y^2}\right) - g\beta\rho(T - T_{\mathrm{ref}}) \tag{7}$$

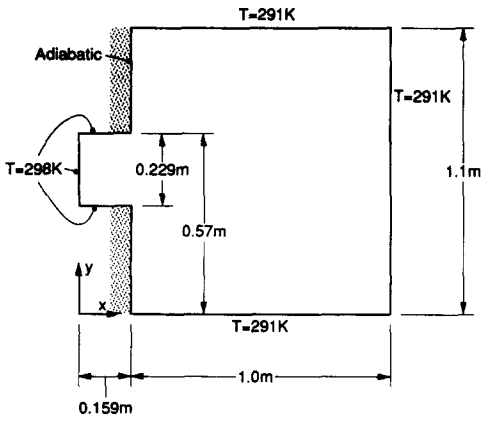

Figure 3 Computational domain and thermal boundary conditions

$$\rho c_p\left(u\frac{\partial T}{\partial x}+v\frac{\partial T}{\partial y}\right)=k\left(\frac{\partial^2 T}{\partial x^2}+\frac{\partial^2 T}{\partial y^2}\right) \tag{8}$$

where the reduced pressure $\hat{p}$ is defined as

$$\hat{p}=p+\rho_{ref}gy \tag{9}$$

and the density is assumed to vary linearly with temperature in the body force term:

$$\rho=\rho_{ref}[1-\beta(T-T_{ref})] \tag{10}$$

with ρ_{ref} and T_{ref} being the density and temperature, respectively, at the reference state. The velocity components, both tangential and normal to the surface, were set to zero at all surfaces, and the thermal boundary conditions were as indicated in Figure 3.

As discussed earlier, the specification of the boundary conditions at "infinity" is an issue that has been resolved in various ways in prior numerical studies of the problem. In general, the predicted velocity and temperature fields within the cavity are insensitive to the precise details of the boundary conditions at "infinity," so long as these boundaries are located far enough away from the cavity. In the present work, the boundaries at "infinity" were taken to be isothermal solid walls. The locations of these boundaries were varied to examine the sensitivity of the computed velocity and temperature fields, and consistent with prior findings, the computed values near and within the cavity were found to be virtually unaffected by the exact location of the far boundaries.

The governing dimensionless parameters of the problem were identified in the usual way, by nondimensionalizing Equations 5–8, and were found to be the Rayleigh and Prandtl numbers and the cavity aspect ratio H/D. For fluids with Prandtl numbers greater than unity, as was the case in the present experiments, it is well known that the Prandtl number ceases to be a significant independent dimensionless group. Thus for a cavity of fixed aspect ratio, the Rayleigh number emerges as the sole governing dimensionless parameter.

The numerical solution procedure was based on the control volume finite-difference scheme described by Patankar,[19] and utilized the power-law approximation to the exponential differencing scheme. The SIMPLER algorithm was used to solve for the velocity components, pressure field, and temperature. The calculations were performed using the dimensional forms of the governing conservation equations (Equations 5–8). Several preliminary computations were conducted to test the sensitivity of the solution to the fineness of the finite-difference grid. These tests provided guidelines in establishing the grids for the final computations. Typically, between 14 and 17 control volume faces in the x direction and between 17 and 19 control surfaces in the y direction were located inside the cavity. The overall numbers of control volume faces in the x and y directions in the domain were 45 and 42, respectively. In order to improve resolution of the velocity and temperature gradients near the walls, control surfaces were closely spaced in the vicinity of the boundaries and were spread farther apart in the middle of the calculation domain. It is estimated that further grid refinement might result in differences on the order of 1 percent in the plate-average and cavity-average Nusselt numbers.

A comment on the use of the exponential differencing scheme in the present calculations is appropriate, as concerns are often raised about the excessive numerical diffusion associated with the scheme. This numerical diffusion arises when the local fluid velocity vector is at an angle to the grid lines, and its magnitude is proportional to the velocity. In the present calculations, substantial flow velocities are encountered mainly in the boundary layers adjacent to the thermally active surfaces. Because these surfaces are aligned with the grid lines, the velocity vectors in the boundary layers are also aligned with the grid lines, and numerical diffusion in these regions is minimal. In the core region, the streamlines do, indeed, cross the grid lines at large angles. However, since the fluid velocity is itself small in the core, once again numerical diffusion is not a significant problem.

Steady-state solutions were obtained for Rayleigh numbers of up to 10^7. Attempts to obtain steady-state solutions at higher Rayleigh numbers were unsuccessful, as the solution oscillated from iteration to iteration. These numerical oscillations, which arise as a consequence of the increasing importance of the inertia terms, have a physical counterpart in the appearance of periodicity in the flow (Chen *et al.*[8]). Computation of the details of the unsteady flow at higher Rayleigh numbers was not attempted owing to the prohibitive expense associated with the requisite fine spatial and temporal resolution of the finite-difference solution. At even higher Rayleigh numbers, the actual flow would be turbulent, and the simulation of such flows would require the incorporation of a suitable turbulence model into the calculation. Such turbulent flow simulations for an open cavity have been presented by Humphrey and To[15] but were not attempted in the present work.

Results

Flow field

The general flow pattern in the computational domain is revealed by the streamlines plotted in Figure 4. These streamlines, which are contours of constant stream function, were obtained from the numerically computed velocity field by defining the dimensionless stream function as:

$$\frac{\partial\psi}{\partial y}=\frac{u}{\nu} \qquad \frac{\partial\psi}{\partial x}=-\frac{v}{\nu} \tag{11}$$

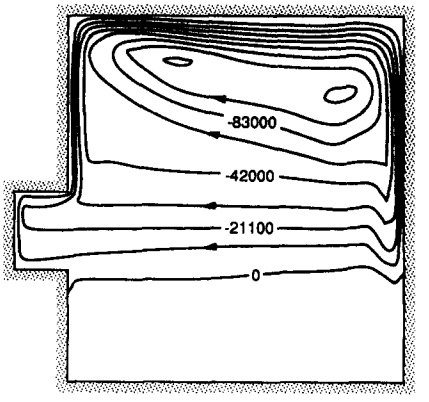

Figure 4 Stream function contours for $Ra_H=10^7$

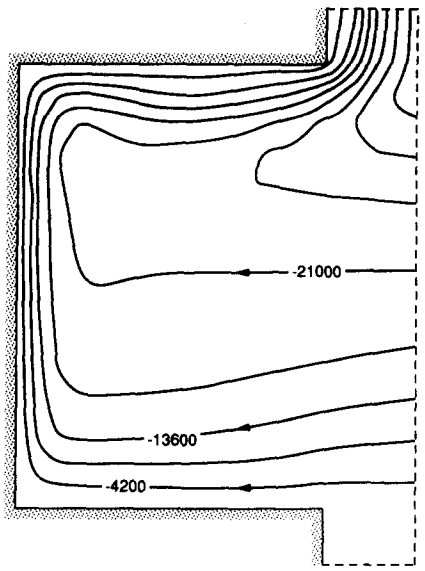

Figure 5 Stream function contours for $Ra_H = 10^7$; close-up view of the cavity

The contours were plotted using a commercial plotting package (DI 3000 from Precision Visuals, Inc.). The package generates contour lines from data on a uniform grid. If, as in this case, the function to be plotted is presented on a nonuniform grid, the program first interpolates values for the plotted function onto a uniform grid superimposed over the nonuniform grid on which the raw data is presented.

The presentation corresponds to the experimental system, which possessed heated cavity walls. To represent the case of cooled cavity walls (as shown in Figure 1) the presentation in Figure 4 would need to be inverted. As shown by the streamlines, flow descending along the cooled wall opposite the cavity opening turns sharply and crosses the domain horizontally to enter the cavity. This fluid penetrates into the cavity before turning and rising along the back wall, turning again towards the cavity opening, and eventually leaving the cavity as a plume of warm fluid. As shown by the zero streamline, there is virtually no flow below the lower lip of the cavity. Details of the computed flow field within the cavity are shown in Figure 5, which is a close-up view of the flow depicted in Figure 4. The boundary-layer character of the flow adjacent to the cavity walls is evident in this close-up view.

Experimental confirmation of the gross features of the predicted flow pattern was obtained in the test cell by direct flow visualization using the thymol blue technique. By positioning the cathode at various locations and observing the motion of the colored streaks, we confirmed that the flow crossed the test cell horizontally at about midheight before entering the cavity, turning, and reemerging as a plume near the upper lip. No flow was observed below the level of the cavity lower lip. It is important to note that, although the gross features of the experimentally observed flow are similar to the predicted flow patterns of Figure 4, there are significant differences. In the experimental study, along the heated back wall of the cavity, the colored streak was rapidly dispersed, suggesting that the flow in the boundary layer might have been turbulent. Indeed, at the Rayleigh number corresponding to the flow visualization studies ($Ra_H = 1.5 \times 10^9$) the back wall boundary layer would be expected to be turbulent.

An even more interesting difference was that, as the flow passed over the lower surface of the cavity, buoyant plumes rose from the surface at various spanwise locations, rendering the flow strongly three-dimensional (3-D). This 3-D configuration could not, of course, be revealed by the 2-D numerical simulation. The flow over the heated bottom surface of the cavity is similar to the classic problem of mixed convection over a heated horizontal surface. The plumes are a result of the instability of the boundary layer on the bottom surface to perturbations of the longitudinal vortex type. Such flows have been studied both experimentally and numerically, and the existence and structure of the 3-D flow have been documented.[20,21]

The visually observed flow patterns are in qualitative agreement with the observations of Chen *et al.*,[9] although there are some differences in detail. A point of similarity between the two studies is that the occurrence of buoyant plumes on the bottom surface of the cavity was also reported by those investigators. However, a notable difference between the two studies lies in the observed flow conditions in the tank below the bottom plane of the cavity. In the present study, the fluid in this region is observed to be almost quiescent while the fluid above the bottom plane flows horizontally into the cavity. In the study by Chen *et al.*,[9] the ambient fluid was observed to flow vertically upward along the wall below the bottom lip of the cavity. This vertical flow then separated at the bottom lip as it turned 90° to enter the cavity. The discrepancy between the present observations and those of Chen *et al.*[9] may be attributed to the fact that, in their studies, the metallic edges of the thick copper plates that constituted the top and bottom walls of the cavity were exposed to the ambient fluid. The buoyancy-driven flow in their study was, therefore, an outcome of not only the heated cavity walls but also the heated metallic edges above and below the cavity entrance. In the present work, the edges of the top and bottom plates are shielded from the ambient fluid by Plexiglas sheets, and the flow is driven solely by the three heated surfaces of the cavity. Consequently, there are qualitative differences between the two studies in the velocity profile in the plane of the cavity opening.

The numerically predicted variation of the horizontal component of velocity at the plane of the cavity opening is plotted for several Rayleigh numbers in Figure 6. The ordinate variable u/u_{max} is the local velocity normalized by the maximum outflow velocity in the cavity opening. Positive values of u are associated with outflow and negative values with inflow. With increasing Rayleigh number, the negative portion of the curve is observed to flatten, and the location of the peak outflow velocity moves upward. The location at which the velocity profile changes sign moves upward from a point only slightly above $H/2$ at $Ra_H = 10^3$ to approximately $0.76H$ at $Ra_H = 10^7$. At $Ra_H = 10^3$,

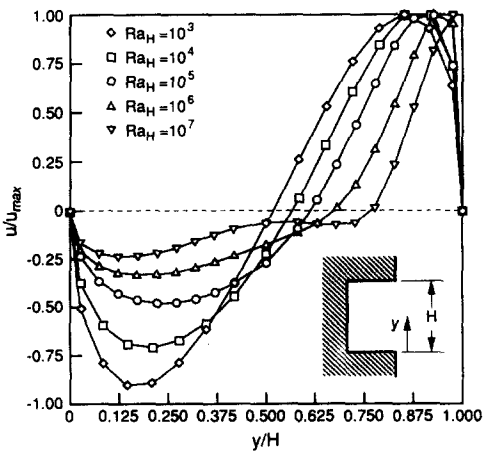

Figure 6 Horizontal velocity component in the plane of the cavity opening

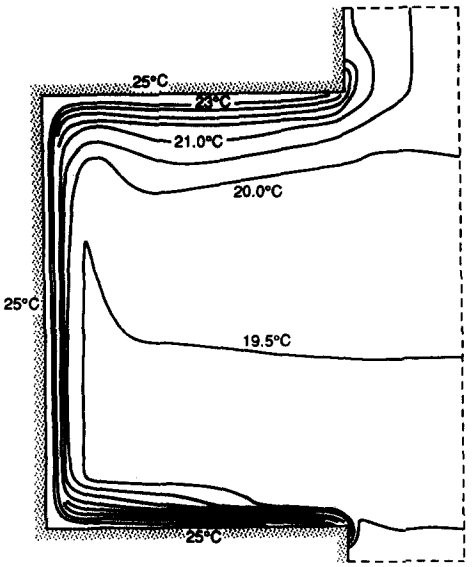

Figure 7 Isotherms inside the cavity for $Ra_H = 10^7$

the maximum velocity entering the cavity is approximately 90 percent of the maximum outflow velocity, whereas for $Ra_H = 10^7$ the maximum inflow velocity is only 23 percent of the maximum outflow velocity. For Rayleigh numbers between 10^4 and 10^7, the maximum outflow velocity is predicted within two percent by:

$$Re_{H,max} = 0.045 Ra_H^{0.53} \tag{12}$$

where $Re_{H,max} = u_{max} H/\nu$.

Temperature field

Numerically predicted temperature variations of the fluid within the cavity are displayed by the isotherms plotted in Figure 7. Local regions of high heat transfer rate along the cavity walls are recognizable by the crowding of the isotherms in those regions. In general, heat transfer at the bottom and back walls of the cavity is seen to be substantially higher than at the top wall.

Local Nusselt numbers

Local variations in the predicted convective heat transfer coefficient are clearly displayed by the plots of the local Nusselt number along the bottom, back, and top surfaces of the cavity in Figures 8, 9, and 10, respectively. The local Nusselt number is defined as:

$$Nu_H = \frac{qH}{\Delta T\, k} \tag{13}$$

with q being the local heat flux. Along the bottom surface, the local Nusselt number is predicted to be highest at the cavity entrance and lowest at the corner between the back and bottom walls (see Figure 8). Close to the cavity entrance, the local Nusselt number varies in a manner consistent with a developing thermal boundary layer in forced convection on a flat plate. Farther along the bottom surface, the local Nusselt number variation is modified by buoyancy effects and the presence of the back wall, which decelerates the flow.

Figure 9 reveals that the local Nusselt number along the back wall is very low at the bottom and top corners and reaches a peak at an intermediate location. Figure 5 provides the explanation for the observed variation. At the two corners, the

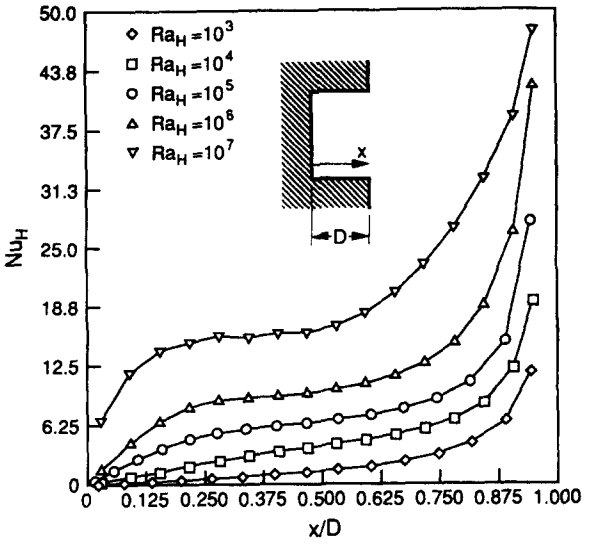

Figure 8 Numerical predictions of the local Nusselt number along the bottom wall of the cavity

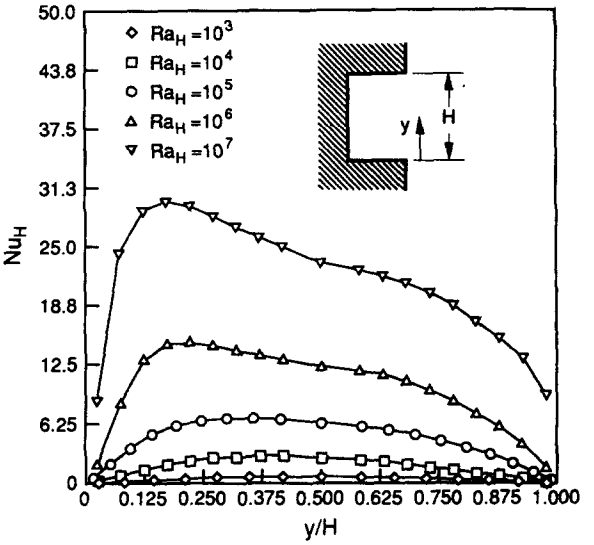

Figure 9 Numerical predictions of the local Nusselt number along the back wall of the cavity

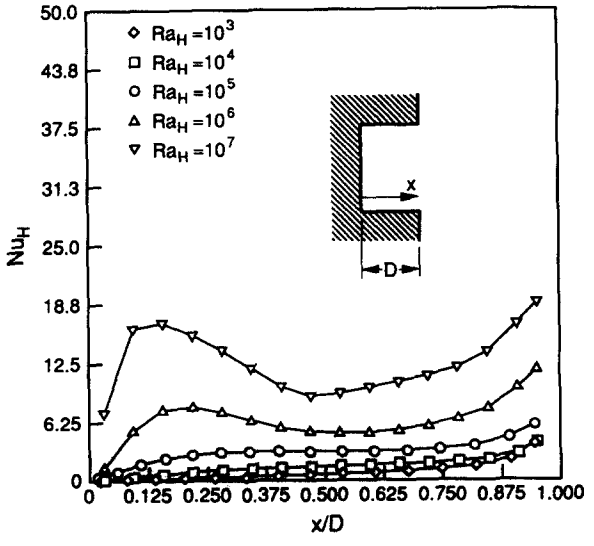

Figure 10 Numerical predictions of the local Nusselt number along the top wall of the cavity

flow speed is low and, correspondingly, the local Nusselt numbers are small. The peak in the Nusselt number distribution corresponds approximately to the height at which the cavity inflow velocity is maximum. This flow impinges on, and is turned by, the back wall, thus yielding high local convection coefficients.

Local Nusselt numbers along the top wall are, on average, smaller than along the back and bottom walls, because the top wall is washed by fluid that has already been heated at the other two surfaces. As displayed in Figure 10, the local Nusselt number is very small near the corner at the back wall, rises to an intermediate peak, diminishes, and eventually rises sharply at the lip of the cavity. The intermediate peak is explained by the impingement and turning of the flow, whereas the sharp rise near the outlet is associated with the acceleration of the flow as it turns the corner under the influence of buoyancy.

Plate-average Nusselt numbers

Comparisons of experimentally measured and numerically predicted plate-average Nusselt numbers for the three surfaces of the cavity are presented in Figures 11, 12, and 13. Comparisons with the numerical predictions of others and empirical correlations for free convection from isolated flat plates also are presented. In presenting comparisons with empirical correlations, the actual Prandtl number corresponding to the experiment is utilized, if required, in the correlations.

Least-squares fits to the numerically predicted and experimentally measured Nusselt numbers have been developed for each of the three surfaces. These correlating equations, which are of the form

$$\overline{Nu}_H = C Ra_H^m \tag{14}$$

are presented in Table 1.

The variation of the surface-average Nusselt number with Rayleigh number is considerably different from plate to plate. Figure 11 shows the variation of the surface-average Nusselt number for the back wall of the cavity. Good agreement between the present numerical predictions and the experimental data is found in the range of Rayleigh numbers where they overlap. For higher Rayleigh numbers, the experimental data fall along an extension of the trend indicated by the numerical predictions.

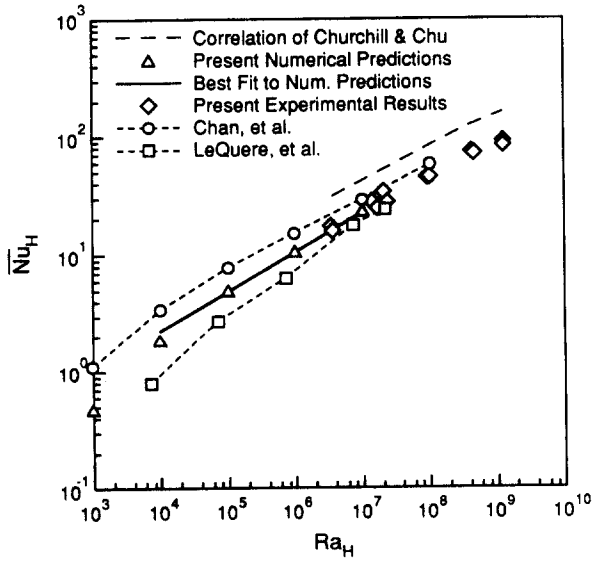

Figure 11 Surface-average Nusselt number for the back wall of the cavity

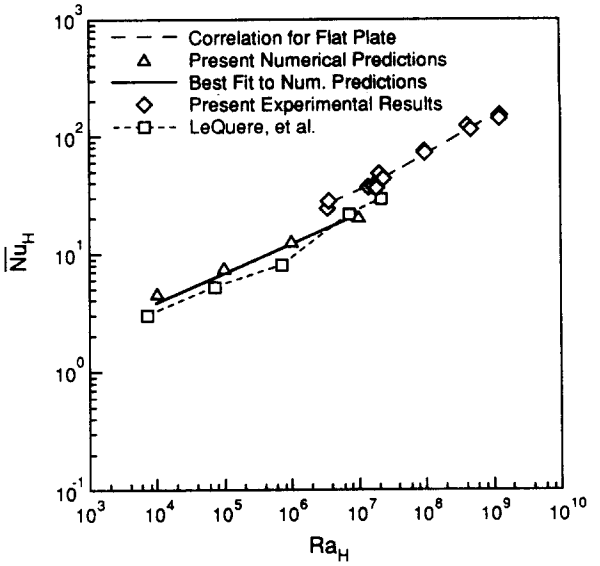

Figure 12 Surface-average Nusselt number for the bottom wall of the cavity

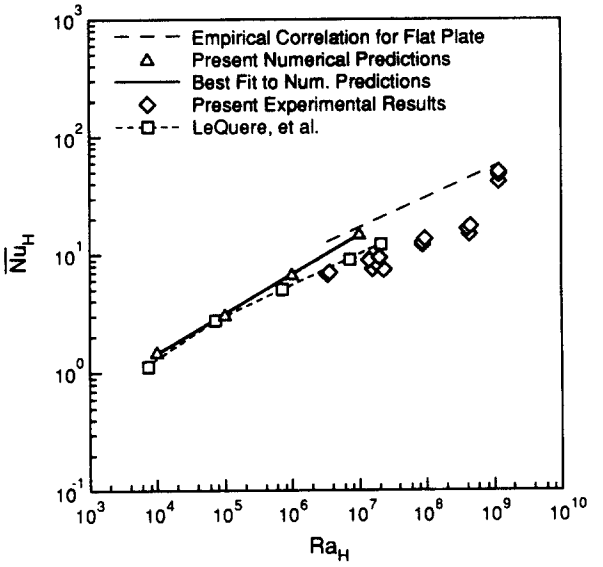

Figure 13 Surface-average Nusselt number for the top wall of the cavity

Table 1 Least-squares fits to the numerically predicted and experimentally measured plate-average Nusselt numbers

Wall	Correlation	Average deviation from data
Numerically predicted Nusselt numbers $10^4 \le Ra_H \le 10^7$		
Back	$0.10 \times Ra_H^{1/3}$	±5%
Bottom	$0.39 \times Ra_H^{1/4}$	±5%
Top	$0.060 \times Ra_H^{1/3}$	±11%
Experimentally measured Nusselt numbers $3.5 \times 10^6 \le Ra_H \le 1.2 \times 10^9$		
Back	$0.086 \times Ra_H^{1/3}$	±8%
Bottom	$0.14 \times Ra_H^{1/3}$	±5%
Top	$0.033 \times Ra_H^{1/3}$	±12%

The least-squares fit to the numerical predictions presented in Table 1 indicates that the predicted plate-average Nusselt numbers vary as the Rayleigh number raised to the power $\frac{1}{3}$. For laminar, external, natural convection heat transfer (such as from a vertical flat plate) the Nusselt number generally correlates with the Rayleigh number raised to the power $\frac{1}{4}$, while the $\frac{1}{3}$ power dependence is typical of turbulent conditions. The $\frac{1}{3}$ power dependence found in the present laminar predictions may be attributed to the impingement of the flow on the back wall of the cavity. This impinging flow is quite different from the type of flow observed adjacent to an isolated vertical flat plate, and a greater sensitivity to the Rayleigh number might be expected.

For free convection from a vertical heated flat plate in an infinite quiescent medium, Churchill and Chu[22] proposed the empirical correlation:

$$\overline{\mathrm{Nu}}_H=\left\{0.825+\frac{0.387\mathrm{Ra}_H^{1/6}}{[1+(0.492/\mathrm{Pr})^{9/16}]^{8/27}}\right\}^2 \tag{15}$$

This correlation plots as a line paralleling the data on Figure 11, but the Nusselt numbers obtained from Equation 15 exceed the data by about a factor of 2. The overprediction of the back wall Nusselt number by the Churchill and Chu correlation could have been anticipated because, as noted earlier, the top and bottom walls impede the vertical flow and thus reduce the heat transfer from the back wall in comparison to that from an isolated vertical plate.

The numerical data of Chan *et al.* and LeQuere *et al.* lie in the vicinity of the present numerical and experimental data. The results of Chan *et al.* exhibit only modest deviations from the present results, despite the fact that those calculations were for the case in which only the back wall was heated. This suggests that local conditions at the back wall are of primary importance to the heat transfer process and that these conditions are not appreciably altered when the top and bottom walls are heated.

In Figure 12, the experimentally determined average Nusselt numbers at the bottom wall are compared with well-known empirical correlations for free convection from a flat plate suspended horizontally in an infinite quiescent medium with the heated surface facing upward. The correlations are

$$\overline{\mathrm{Nu}}_L=0.54\mathrm{Ra}_L^{1/4} \tag{16}$$

for Rayleigh numbers in the range $10^4\le \mathrm{Ra}_L\le 10^7$ and

$$\overline{\mathrm{Nu}}_L=0.15\mathrm{Ra}_L^{1/3} \tag{17}$$

for Rayleigh numbers in the range $10^7\le \mathrm{Ra}_L\le 10^{11}$, according to Incropera and DeWitt.[23] The characteristic length recommended for use with this correlation is calculated from the surface area A_{plate} and the perimeter of the plate P_{plate}, so that:

$$L=\frac{A_{\text{plate}}}{P_{\text{plate}}} \tag{18}$$

As the situation for which the empirical correlation has been developed is markedly different from the one encountered in the present experiment, the characteristic length used here is determined differently. In the case of the horizontally suspended flat plate, the fluid can flow freely over all four edges of the plate. In the present experiment, only one edge, at the front of the cavity, allows this free flow. This is the case for both the bottom and top surfaces of the cavity. On two sides and at the back, the vertical walls of the cavity restrict such flow. Hence, instead of the total perimeter of the plate, only the length W of the cavity lip is used. Therefore

$$L=\frac{A_{\text{plate}}}{W} \tag{19}$$

This characteristic length is different from the one used to determine the Rayleigh and Nusselt numbers for the experimental and numerical data, so the two correlations (Equations 16 and 17) need to be changed accordingly. $\overline{\mathrm{Nu}}_L$ and Ra_L can be expressed in terms of $\overline{\mathrm{Nu}}_H$ and Ra_H, respectively:

$$\overline{\mathrm{Nu}}_L=\frac{L}{H}\times\overline{\mathrm{Nu}}_H \tag{20}$$

$$\mathrm{Ra}_L=\frac{L^3}{H^3}\times\mathrm{Ra}_H \tag{21}$$

Substitution of these expressions into Equations 16 and 17 results in

$$\overline{\mathrm{Nu}}_H=0.54\times\left(\frac{H}{L}\right)^{1/4}\times(\mathrm{Ra}_H)^{1/4} \tag{22}$$

for the range of Rayleigh numbers

$$\left(\frac{H}{L}\right)^3\times 10^4\le \mathrm{Ra}_H\le\left(\frac{H}{L}\right)^3\times 10^7$$

and

$$\overline{\mathrm{Nu}}_H=0.15\times\mathrm{Ra}_H^{1/3} \tag{23}$$

for

$$\left(\frac{H}{L}\right)^3\times 10^7\le Ra_H\le\left(\frac{H}{L}\right)^3\times 10^{11}$$

In this form, the empirical correlations yield Nusselt numbers that are essentially coincident with the experimental data (see Figure 12). The adjustment of the characteristic length in the empirical correlations sufficed to make them predict the heat transfer at the bottom plate with very good accuracy. This rather surprising fact suggests that the flow and heat transfer conditions for the bottom plate are not appreciably influenced by the presence of the other heated surfaces of the cavity. The least-squares fit to the experimental data (Table 1) is very close to Equation 23.

The numerically determined Nusselt numbers for the bottom plate are lower than both the experimental and the empirical values, and also increase more slowly with Ra_H. A likely explanation for this is the inability of the present numerical formulation to capture the 3-D nature of the flow above the bottom plate. In the flow visualization experiments, mushroom-shaped plumes of hot fluid could be observed rising from the bottom plate and being slowly swept along with the flow. These plumes are distinctly 3-D phenomena that cannot be simulated by the 2-D formulation used for the numerical modeling. Their existence increases heat transfer from the bottom plate, thus raising the Nusselt number.

For the top plate, the comparison between the numerical and experimental results and the empirical correlation is markedly less favorable (Figure 13). The empirical correlation for a hot horizontal surface facing downward, or a cold surface facing upward, is

$$\overline{\mathrm{Nu}}_L=0.27\times\mathrm{Ra}_L^{1/4} \tag{24}$$

for the range of Rayleigh numbers of $10^5\le \mathrm{Ra}_L\le 10^{10}$, which can be transformed to

$$\overline{\mathrm{Nu}}_H=0.27\times\left(\frac{H}{L}\right)^{1/4}\times\mathrm{Ra}_H^{1/4} \tag{25}$$

for

$$\left(\frac{H}{L}\right)^3\times 10^5\le \mathrm{Ra}_H\le\left(\frac{H}{L}\right)^3\times 10^{10}$$

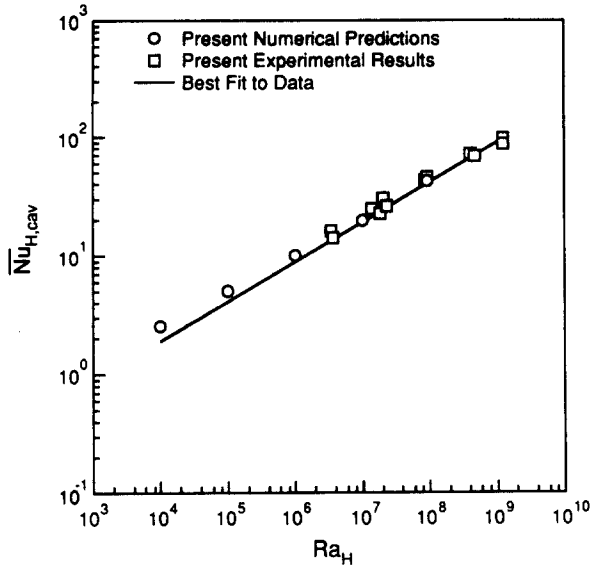

Figure 14 Cavity-average Nusselt number

The experimental results start at a level somewhat below that of the numerical results (roughly half as large as the values predicted by the empirical correlation) and, at first, rise more slowly with increasing Rayleigh number up to $Ra_H = 5.0 \times 10^8$. At that value of Ra_H they are almost three times smaller than the empirical correlation. Above that, the measured Nusselt number increases much faster than before and almost reaches the value predicted by the empirical correlation. As discussed earlier, the uncertainty in determination of the Nusselt number at the top plate is significant at low Rayleigh numbers. The observed deviations between the experimental data and the numerical predictions may be attributed partly to these uncertainties.

The various numerical predictions differ from each other, from the empirical correlation, and from the experimental results. While the predictions by LeQuere *et al.* display the same behavior as the predictions for the other plates, the predictions of this study show a stronger dependence of the Nusselt number on the Rayleigh number.

The significant difference between the present data and the empirical correlation for a heated horizontal flat plate suggests that the heat transfer conditions at the top plate are most strongly influenced by the presence of the two other heated plates. The heat transfer coefficient at the top plate is substantially lower than that predicted by the use of the empirical correlation because the surface is washed by fluid heated by the bottom and back plates. If the walls of the cavity are cooler than the ambient fluid, the present results for the bottom plate would then apply to the top plate and vice versa.

Numerical predictions and experimental data are in good agreement in the case of the cavity-average Nusselt number (Figure 14). A single correlation was fit to both sets of data, covering the range of Rayleigh numbers between 10^4 and 1.2×10^9. The correlation was found to be

$$\overline{Nu}_{H,cav} = 0.087 \times Ra_H^{1/3} \tag{26}$$

with an average deviation between the correlation and the data of 8 percent. Clausing[3] presented the following empirical correlation for the cavity average Nusselt number based on experiments with high temperature solar central receiver cavities:

$$\overline{Nu}_{H,cav} = 0.082 \times Ra_H^{1/3}\left[-0.9 + 2.41\left(\frac{T_w}{T_\infty}\right) - 0.5\left(\frac{T_w}{T_\infty}\right)^2\right] \tag{27}$$

for

$$Ra_H > 1.6 \times 10^9 \quad \text{and} \quad 1 < \frac{T_w}{T_\infty} < 2.6$$

This correlation is in excellent agreement with the present results; it differs by no more than 2 percent from the best fit line of Equation 26. The numerical predictions of Humphrey and To[15] for the cavity-average Nusselt number are also in very good agreement with the present results. For $Ra_H \approx 3 \times 10^7$, their predicted value of $\overline{Nu}_{H,cav}$ is 27.3 and Equation 26 yields 27.0.

Conclusions

A combined numerical and experimental study of natural convection in a side-facing open cavity was conducted. The flow and temperature fields were computed and displayed through streamline and isotherm contour maps. Significant variations in the local Nusselt numbers along the cavity surfaces were predicted, these variations being correlated to features of the flow field. Correlating equations for the experimentally determined surface-average and cavity-average Nusselt numbers were developed in terms of a Rayleigh number based on the height of the cavity, the Rayleigh number ranging between 3.5×10^6 and 1.2×10^9. The surface-average Nusselt number for the back wall was found to be in qualitative agreement with an existing empirical correlation for an isothermal vertical plate, but was overpredicted by the correlation. For the bottom plate, good quantitative agreement was obtained between the experimental results and an existing empirical correlation for an isothermal horizontal flat plate. Agreement between the data and the existing correlation was relatively poor for the top plate. The numerical predictions, which covered the Rayleigh number range from 10^3 to 10^7, were in good agreement with experimental data for the back plate, underpredicted the data for the bottom plate, and overpredicted the top-plate data.

References

1 Boehm, R. F. A review of convective loss data from solar central receivers. *J. Solar Energy Eng.*, 1987, **109**, 101–107
2 Siebers, D. L., Abrams, M., and Gallagher, R. J. Solar thermal central receivers, ASME Paper No. 79-WA/HT-38, 1979
3 Clausing, A. M. Convective losses from cavity solar receivers—comparison between analytical predictions and experimental results. *J. Solar Energy Eng.*, 1983, **105**, 29–33
4 Kraabel, J. S. An experimental investigation of the natural convection from a side-facing cubical cavity. *Proc. ASME–JSME Thermal Energy Joint Conf.*, 1983, **1**, 299–306
5 Chan, Y. L. and Tien, C. L. Laminar convection in shallow open cavities. *J. Heat Transfer*, 1986, **108**, 305–309
6 Hess, C. F. and Henze, R. H. Experimental investigation of natural convection losses from open cavities. *J. Heat Transfer*, 1984, **106**, 333–338
7 Sernas, V. and Kyriakides, I. Natural convection in an open cavity. *Proc. 7th Int. Heat Transfer Conf.*, 1982, **2**, 275–286
8 Chen, K. S., Humphrey, J. A. C., and Miller, C. Note on the pulsating nature of thermally driven open cavity flow. *Int. J. Heat Mass Transfer*, 1983, **26**, 1090–1093
9 Chen, K. S., Humphrey, J. A. C., and Sherman, F. S. Free and mixed convective flow of air in a heated cavity of variable rectangular cross section and orientation. *Phil. Trans. R. Soc. Lond.*, 1985, **A316**, 57–84
10 Chan, Y. L. and Tien, C. L. A numerical study of two-dimensional natural convection in square open cavities. *Numer. Heat Transfer*, 1985, **8**, 65–80
11 Chan, Y. L. and Tien, C. L. A numerical study of two-dimensional laminar natural convection in shallow open cavities. *Int. J. Heat Mass Transfer*, 1985, **28**, 603–612

12 Penot, F. Transfert de chaleur par convection naturelle dans une cavite rectangulaive isotherme ouverte sur une face. *Revue Phys. Appl.*, 1980, **15**, 207–212
13 Penot, F. Numerical calculation of two-dimensional natural convection in isothermal open cavities. *Numer. Heat Transfer*, 1982, **5**, 421–437
14 LeQuere, P., Humphrey, J. A. C., and Sherman, F. S. Numerical calculation of thermally driven two-dimensional unsteady laminar flow in cavities of rectangular cross section. *Numer. Heat Transfer*, 1981, **4**, 249–283
15 Humphrey, J. A. C. and To, W. M. Numerical simulation of buoyant turbulent flow—II. Free and mixed convection in a heated cavity. *Int. J. Heat and Mass Transfer*, 1986, **29**, 593–610
16 Miner, C. S. and Dalton, N. N. (Eds.) *Glycerol*. Reinhold, New York, 1953.
17 Skok, H. Buoyancy driven flow and heat transfer in a side-facing open cavity with application to heat transfer in a household refrigerator. M.S.M.E. thesis, Purdue University, 1988
18 Sparrow, E. M., Chrysler, G. M., and Azevedo, L. F. Observed flow reversals and measured-predicted Nusselt numbers for natural convection in a one-sided heated vertical channel. *J. Heat Transfer*, 1984, **106**, 325–332
19 Patankar, S. V. *Numerical Heat Transfer and Fluid Flow*. Hemisphere/McGraw-Hill, Washington, 1980
20 Knox, A. L. and Incropera, F. P. Mixed convection flow and heat transfer in the entry region of a horizontal rectangular duct, Paper 86-HT-18, AIAA/ASME Thermophysics and Heat Transfer Conf., 1986
21 Mahaney, H. V., Incropera, F. P., and Ramadhyani, S. Development of laminar mixed convection flow in a horizontal rectangular duct with uniform bottom heating. *Numer. Heat Transfer*, 1987, **12**, 137–155
22 Churchill, S. W. and Chu, H. H. S. Correlating equations for laminar and turbulent free convection from a vertical flat plate. *Int. J. Heat and Mass Transfer*, 1975, **18**, 1323–1339
23 Incropera, F. P. and DeWitt, D. P. *Fundamentals of Heat and Mass Transfer*. John Wiley & Sons, New York, 1985